Authors: Mujahid Ahmed, Noah Lopez, Pulkit Rustagi
Topic: Stress Analysis of Bicycle Wheel Given Variations in Lacing Pattern and Spoke Count
Course: ME471/AE420 - Finite Element Analysis

Introduction:

As an integral part of a bicycle, wheels tend to have a large impact both on the design and performance for its discipline. In the Mountain Biking discipline, the wheel will be more "flexible" allowing the bike to absorb impacts more easily, while in the Road Biking discipline, the wheel will be very stiff to allow for better power transfer between the rider and the ground. The goal of this project is to develop a rudimentary wheel stress and deflection FEM solver accounting for three different lacing patterns, and a completely variable number of spokes under various loading conditions.

In industry, this analysis would take place through real-world testing of new designs, as well as through simulations in the company's chosen FEA/CAD package. Those packages, such as Dassault SolidWorks, PTC Creo, and Ansys, are able to create and solve dimensionally accurate meshes providing a solution within a given percentage of the real-world testing outcomes. They are also able to provide animations of the deflection for better visualization, finer meshes in areas with localized stresses, and many more options.

However, before an engineer is able to effectively use one of those software packages, they must understand what is required to solve their problem. Without an understanding of the system, an engineer could fall victim to a "Garbage In, Garbage Out" situation leading to, possibly, catastrophic flaws in their designs.

Background:

Intuitively thinking, the most stressed location on the wheel would be the bottom, where the tire contacts the ground and bumps are absorbed. However, this is not the case. In fact, it is the exact opposite due to the structure of the connections between the rim, spokes, and hub. Since the spokes are held in place under tension between the rim and hub, as the wheel rolls, the tension only decreases on the lower spokes and increases on the upper spokes. This is a limitation in our solution however, as we consider the spokes to be firmly attached to the rim with no way to transfer the compression in the lower spokes to tension in the upper spokes and no pretension in the system.

Another common occurrence in poorly maintained bicycles is a spoke failure. Our solution is able to simulate the loss of a spoke both at the top or at the bottom of the wheel. By then varying the parameters of our system, we are able to design an optimal wheel that can withstand the forces exerted while the bike is being ridden.

Problem Formulation, Geometry, and Assumptions:

Since the structure of a wheel varies between different bicycles as well as between the front and rear wheels, a flexible solver was required. The flexibility in our solution begins with the node mapping function that pulls the requested pattern and number of spokes. Based on the defined parameters, it is able to calculate the required spoke connections between the hub and rim. While very straight forward with 2-node rim elements, this was made more complicated by the use of 3-node parabolic elements allowing for an increase in accuracy of our system.

Assuming equiangular spacing between each node on the hub, as well as the rim, the mapping function determines their locations via polar coordinates and then converts them to the global *(x, y)* axes. Of note is that the rim nodes are spaced at half the angle change as the hub nodes due to the 3-node elements. An example of this can be seen below for a radial, 8 spoke wheel in Figure 1. As is easy to see, for an 8 spoke wheel, there will be a 45 degree angle between each node on the hub, and only 22.5 degrees between each node on the rim. This way of mapping allows our plotting function to easily adapt to changes in wheel structure.

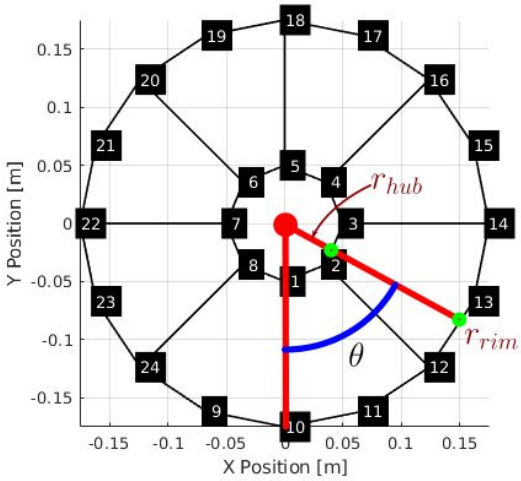

Figure 1 (Left) : *An example showing the polar mapping of nodes to (x, y) coordinates as well as numbering scheme*

In a non-radial spoke lacing pattern, the nodes are numbered identically as a radial pattern. However, the spokes connecting between the hub nodes and rim nodes are no longer straight but rather in a crossing pattern, hence the name, “1/2/3-cross”. These crossing patterns require an even number of spokes and offset ±2 x # crosses resulting in the patterns seen below in Figure 2.

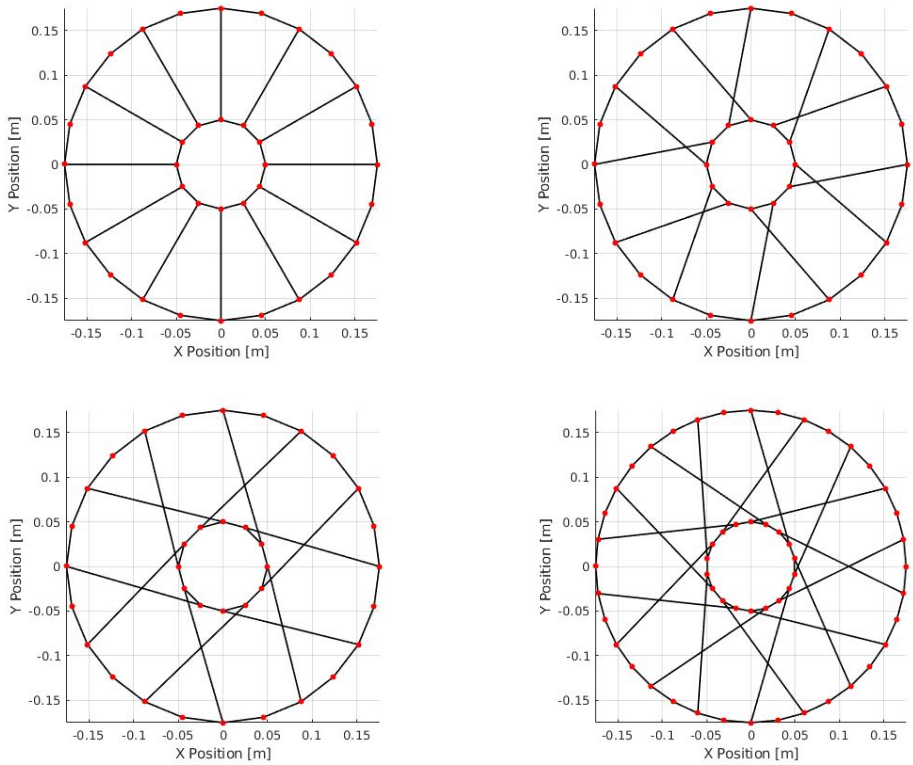

Figure 2: Each crossing pattern (radial, 1-cross, 2-cross, 3-cross)

The group opted to use the variational approach to formulate the finite element method for this problem. Starting with the potential energy function

$$\Pi = U + V = EA \iint_S ((\frac{\partial u}{\partial x})^2 + (\frac{\partial u}{\partial y})^2)\partial S - \iint_S f * u(x,y)\partial S \tag{1}$$

Where *u* is the displacement field, *S* is the surface of the structure, and f is an applied point force. From Equation 1, we substitute in the shape functions to create the basic approximation form of the potential energy function for an individual element within a finite element mesh, shown below in matrix form.

$$\tilde{\Pi^e} = EA \iint_{S_e} \langle d \rangle [B]' [B] \partial S_e \{d\} - \iint_{S_e} f \langle N \rangle \partial S_e \tag{2}$$

Where *B* is defined as the matrix composed of the derivative shape functions, *d* is the displacement vector, *N* is the matrix of shape functions, and *Se* is the surface of a single element. From here, the group needed to determine the shape functions and stiffness matrices for both types of elements present in the wheel model. The spokes of the wheel were treated as 2d truss elements as they were bars with only 2 nodes at each endpoint, which vastly simplified the calculations required in the problem. For any given 2d truss element, the stiffness matrix k is given as

$$[k^e] = \frac{EA}{l} \begin{bmatrix} c^2 & cs & -c^2 & -cs \\ cs & s^2 & -cs & -s^2 \\ -c2 & -cs & c^2 & cs \\ -cs & -s^2 & cs & s^2 \end{bmatrix} \tag{3}$$

Where c stands for the cosine of the angle the spoke makes with the hub defined from the hub and s stands for the sine of the same angle. One thing to note is that this stiffness matrix required no integration to calculate, so computational time was quite fast.

The rims were modeled as 3 node elements with the center node being attached to a spoke and the other two nodes being halfway to the next spoke. The group took two approaches when it came to modeling the rims. The first approach was to simply split each 3 node element into 2 2d truss elements, much like the spokes. This was done to get a loose approximation of the solution and ensure all the pieces of the solver worked together to provide a coherent solution. The stiffness matrix for a 2d truss rim element was the same as the one given in Equation 3.

The second method of modeling the rim involved using a 2d 3-node cable element. The shape functions for this element were troublesome to find, however the group eventually found an fea research paper published from Chongqing University in 2009 (Liu 2009) [1] . This paper went over the fea formulation of an overhead electrical transmission line and laid their FEM formulation very clearly. This leads to the following base element shown in Figure 3 and shape functions, both of which were taken directly for the Chongqing paper.

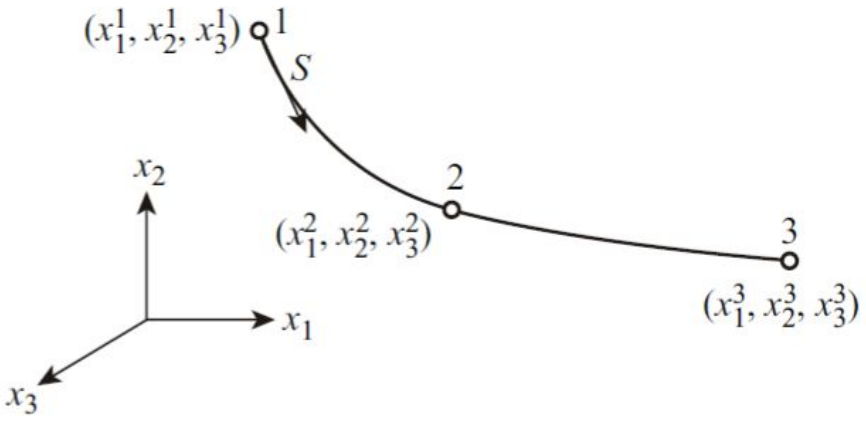

Figure 3: Depiction of base element used in integration of rim stiffness matrix

$$N_1 = \frac{2S^2}{l_e^2} - \frac{3S}{l_e} + 1, N_2 = \frac{-4S^2}{l_e^2} - \frac{S}{l_e}, N_3 = \frac{2S^2}{l_e^2} - \frac{S}{l_e} \tag{4}$$

Where S is the location along the element ranging from 0 to the length of the element, *le*. As noted the shape functions are one dimensional and given in terms of *S*. As a result, the shape functions were initially converted into polar coordinates.

$$S = r\Theta$$
$$\langle\Theta\rangle = \langle\Theta_1, \Theta_2, \Theta_3\rangle \tag{5}$$

Where r is the polar location along the element, a constant dictated by the spokes, and theta is defined as the angle between one node on the element and the rim, split up into a vector for each node. Converting the shape functions into polar yields

$$N = \left[\frac{2(r\Theta)^2}{l_e^2} - \frac{3r\Theta}{l_e} + 1, \quad \frac{-4(r\Theta)^2}{l_e^2} - \frac{r\Theta}{l_e}, \quad \frac{2(r\Theta)^2}{l_e^2} - \frac{r\Theta}{l_e}\right] \tag{6}$$

In order to compute the stiffness matrix in cartesian coordinates, the group calculated the derivative of the shape functions with respect to x and y coordinates using the chain rule

$$\frac{\partial N}{\partial x} = \frac{\partial N}{\partial r} * \frac{\partial r}{\partial x}$$
$$\frac{\partial N}{\partial r} = r * (\langle\Theta\rangle \cdot \langle N\rangle), \frac{\partial r}{\partial x} = \frac{1}{cos(\Theta)}$$
$$\frac{\partial N}{\partial x} = \frac{r}{cos(\Theta))} * (\langle\Theta\rangle \cdot \langle N\rangle)$$

$$\frac{\partial N}{\partial y} = \frac{r}{sin(\Theta)} * (\langle \Theta \rangle \cdot \langle N \rangle) \tag{7}$$

Additionally, the group required the resulting Jacobian of this coordinate transform to use in the following integration.

$$det(J) = \frac{\partial (r * (\langle \Theta \rangle \cdot \langle N \rangle))}{\partial S} \tag{8}$$

From Equation 6, the group was able to derive the element wise B matrix for the cable element and used a 3-point Guassian quadrature integration to finally arrive at the elemental stiffness matrix for the rim.

$$B_{quadratic} = \begin{bmatrix} \frac{\partial N_1}{\partial x} & 0 & \frac{\partial N_2}{\partial x} & 0 & \frac{\partial N_3}{\partial x} & 0 \\ 0 & \frac{\partial N_1}{\partial y} & 0 & \frac{\partial N_2}{\partial y} & 0 & \frac{\partial N_3}{\partial y} \\ \frac{\partial N_1}{\partial x} & \frac{\partial N_1}{\partial y} & \frac{\partial N_2}{\partial x} & \frac{\partial N_2}{\partial y} & \frac{\partial N_3}{\partial x} & \frac{\partial N_3}{\partial y} \end{bmatrix} \tag{9}$$

Finally obtaining the B matrix allows for the formulation of the elemental stiffness matrix for the 3-node cable element defined as,

$$[k^e] = \frac{EA}{l_e} * \int_{x_a}^{x_b} \int_{y_a}^{y_b} \{B\} * [B] * det(J) \partial x \partial y \tag{10}$$

As can be seen in Equation 7, when converting from polar coordinates to cartesian, it is possible to approach a divide-by-zero situation. To avoid this, the group added an offset of 0.1 radians to the positioning of the rim's elements held in the theta matrix.

$$\langle \Theta \rangle' = \langle \Theta \rangle + \Phi \tag{11}$$

Where phi is a small angle offset. This offset was tested and observed to have no significant impact on the results of the simulation and proved to be a very simple way to avoid dividing by zero.

Loading and Boundary Conditions:

A standard bicycle wheel tends to have steel hub and spokes, an aluminum rim, and a rubber tire[1]. The most common type of wheel has a rim 26" in diameter with a width of approximately 1". If an average rider weighs 180lbs, and their weight distribution on the bike is split 60 rear / 40 front, a load of approximately 108lbs can be found at the rear and 72lbs at the front. Upon hitting a bump, these loads could spike up to twice that. Since the hub tends to be much stronger and stiffer than the spokes, we have assumed that there will be no deflection of the nodes defining the boundary of the hub. See Tables 1 and

[1] We opted not to simulate the tire due to the non-linear properties of deflection with rubber material.

2, below, for a list of material specifications as well as the boundary conditions mentioned above. Figure 4, below, depicts the three loading conditions we chose on the 1-cross patterned wheel.

Table 1: Item Properties

	Hub	**Spokes**	**Rim**
Material	Stainless Steel	Stainless Steel	Aluminum
Density (ρ, *kg/m^3*)	7600	7600	2700
Young's Modulus (*E, pa*)	190 x 10^9	190 x 10^9	70 x 10^9
Count	1	3 -- 36 (Pattern Dependent)	1
Length (*m*)	*N/A*	0.30	*N/A*
Width (*m*)	*N/A*	*N/A*	0.025
Diameter (*m*)	0.10	0.002	0.70

Table 2: Loading and Boundary Conditions

	Hub	**Spokes**	**Rim**
Fixed DoF	All	N/A	N/A
Preload (*N*)	0	0	0
Point Loads	No	No	Yes
Distributed Loads	No	No	Yes
Force Magnitudes (*N*)	N/A	N/A	300 -- 800

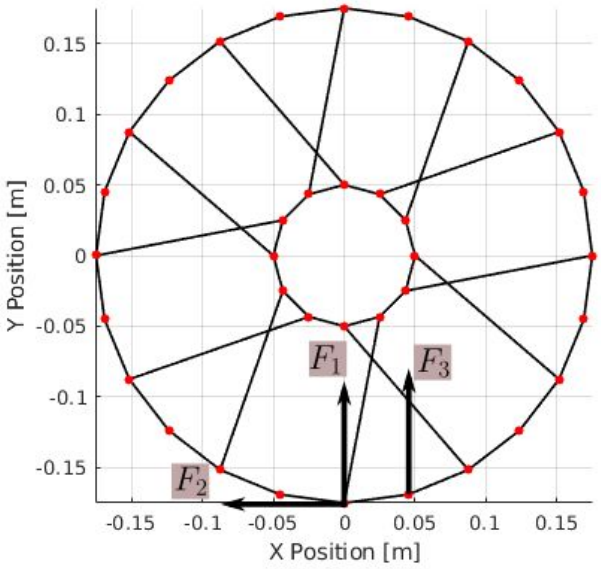

Figure 4: Depiction of Loading Conditions for our Solution

All loading conditions can be assumed to be 300N unless otherwise specified. The first loading condition correlates to ideal riding conditions on a perfectly smooth surface with constant load. The second correlates to hitting a bump in the road. The third simulates a braking load. This situation would be seen specifically with brakes located at the rim rather than disc or hub-based brakes. In the event of brakes located near the center of the wheel, there is a much larger torsion load applied. In the event that a radially laced wheel had a hub-based brake, the wheel would collapse upon heavy and possibly even light braking.

Results:

Below are the results from our FEM solver based on a variety of parameters. We first looked at the three different loading conditions (F1, F2, and F3) and compared the deflection of the wheel given different lacing patterns. Next, we determined the location of the maximum deflection as well as the actual deflection values at that position. Third, using the 1-cross pattern and F1 loading condition, we varied the number of spokes comparing both the maximum *x* and the maximum *y* deflections. Finally, we calculated the stress at each node, using the F1 loading condition with a radially laced wheel.

Table 3: Max Deflections (in mm) for each loading condition with 12 spokes [Node #, dx, dy].
Note 1: Per loading condition the deflections are identical
Note 2:Node 15 is one node forward of the lowest point on wheel

	F1	**F2**	**F3**
Radially Laced	[15, -1.20e-8, 9.39e-8]	[15, -1.18e-7, -1.99e-8]	[15, 6.85e-8, 3.57e-7]
1-Cross Pattern	[15, -1.20e-8, 9.39e-8]	[15, -1.20e-8, 9.39e-8]	[15, 6.85e-8, 3.57e-7]
2-Cross Pattern	[15, -1.20e-8, 9.39e-8]	[15, -1.20e-8, 9.39e-8]	[15, 6.85e-8, 3.57e-7]

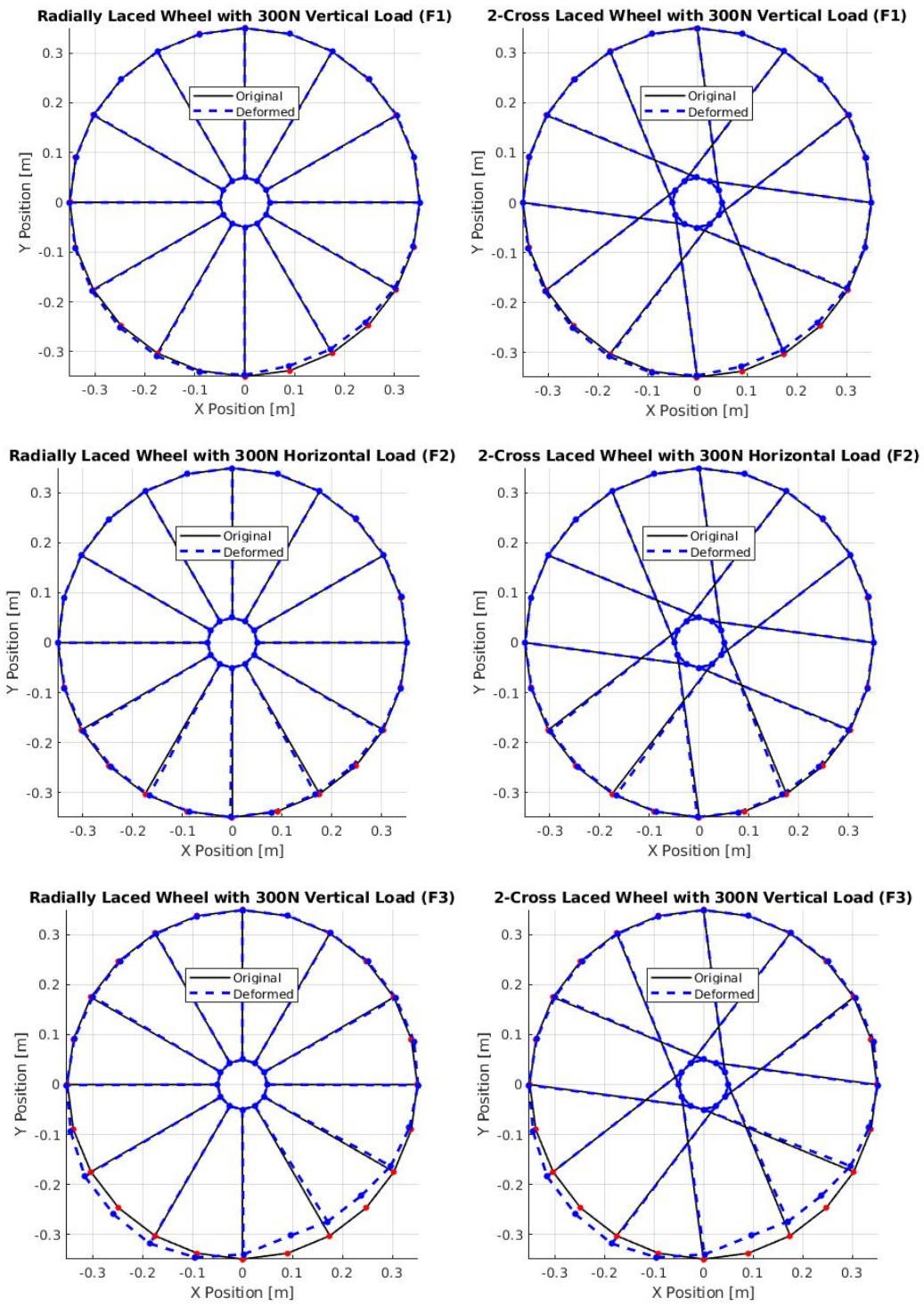

Figure 5: Deflection comparisons given different loading conditions with 12 spokes

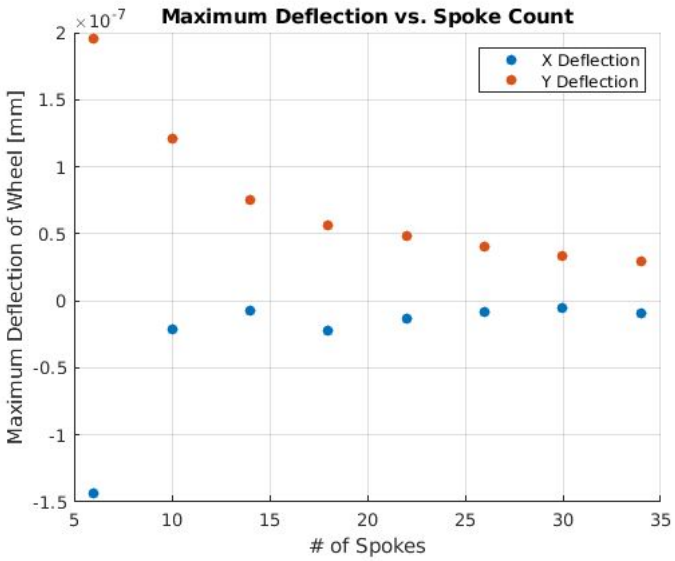

Figure 6: Maximum deflections (in mm) for 1-cross spoke pattern in F1 loading condition with varying spoke count

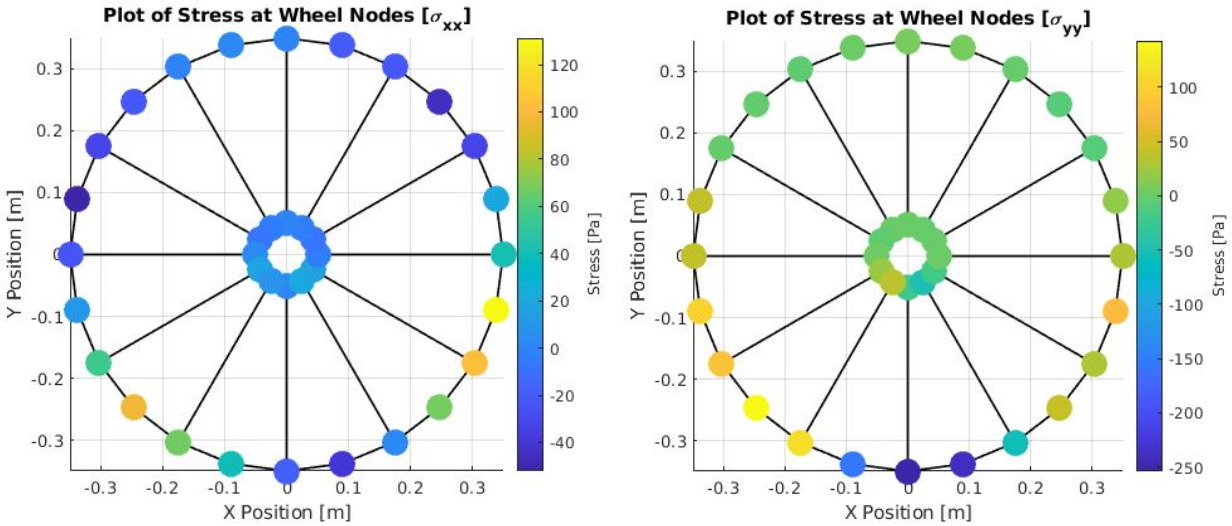

Figure 7: Plot of Stresses in Wheel During F1 Loading Conditions

Convergence

Normally, a convergence test would be run to see how the maximum deflection of any node changes with the number of elements and nodes in a mesh. However, the way the group linked the number of spokes with the number of elements means that this wouldn't be a conclusive test, as the actual stiffness of the wheel would increase with each additional element, spoke added. As a result, the group has opted to plot the performances of using a linear truss element model for the rim versus a quadratic cable element. As previously mentioned however, the resulting global stiffness matrix from using the linear truss rim element was extremely unstable and threw many singularity warnings within matlab, making the data from those simulations incredibly erratic. That being said, Figure 6 depicts the maximum vertical deflection as a function of the number of spokes in the 1-cross wheel configuration using either the quadratic rim or linear rim.

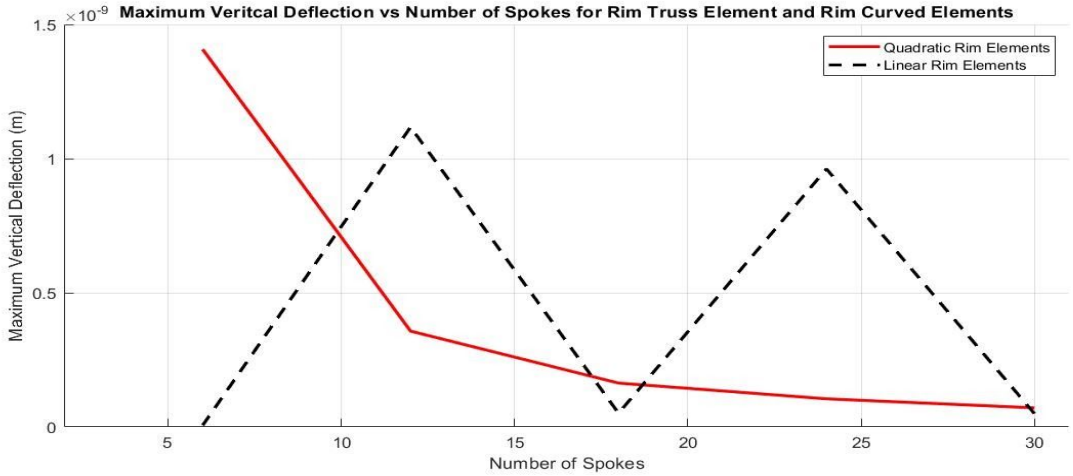

Figure 8: Plot comparing the performance of linear rim elements and quadratic rim elements

As mentioned above, the linear rim behaviour is very strange and can mostly be accounted for by the discontinuities caused by using a linear element to simulate a circular bike wheel. The quadratic rim behaves much nicer, displaying predicted behaviour as the maximum deflection decreases while the both the element count and the physical stiffness of the wheel increases, somewhat implying that the group's solver does converge to answer. However, as stated this is unfortunately not incredibly conclusive as the stiffness of the wheel increases with the number of elements.

Improved Design:

As can be seen in Table 3 in the results, the radial stiffness of the wheel is not changed by introducing a crossing pattern during spoke lacing. However, as seen in Figure 6, the number of spokes used greatly affects the stiffness of the wheel. In our improved design, we are targeting a very stiff wheel for a road bicycle with a starting point of a 12 spoke radially laced wheel.

On a normal wheel, there may be up to 36 spokes. In light weight wheels, there can be as low as 24 spokes. However, there are types of wheels that are a solid disk providing both aerodynamic and stiffness benefits. This can be seen in our improved design that contains 100 spokes, which converges on an equivalent stiffness of a solid disk while still being lighter due to the radial lacing pattern. Figure 9, below, shows a comparison of our initial and improved designs. This figure also lends to what was mentioned previously about the convergence of our model. As we increase the number of spokes in our model, the number of nodes on the rim increases by a factor of 2. This leads to a more uniform distribution of deflection and therefore stress in our system.

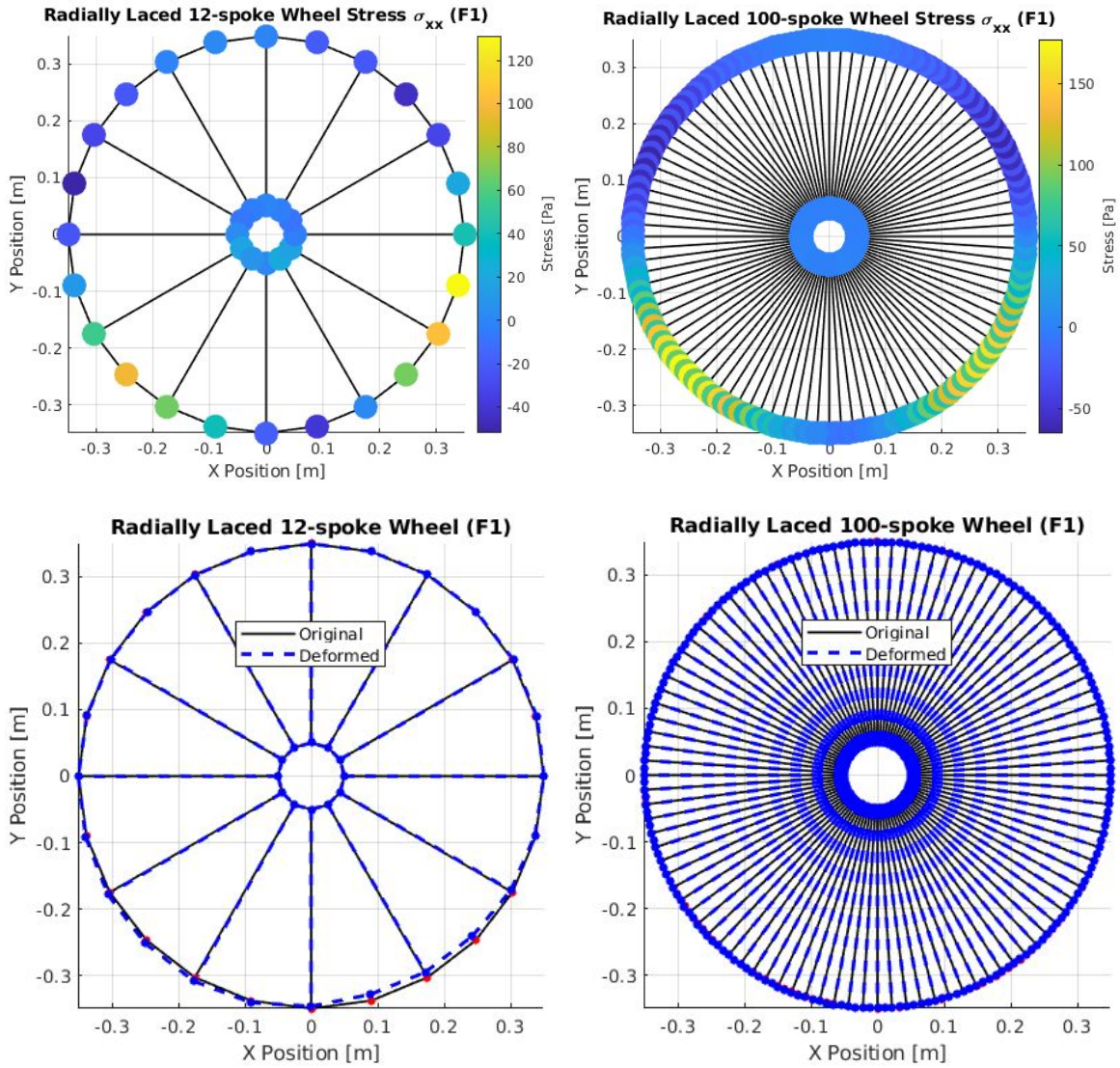

Figure 9: Plot of Stress and Deflections Comparing Wheel Designs

Discussion and Conclusion:

In running our simulation we proved a couple hypotheses of ours wrong. Firstly, we expected that the wheels with crossing patterns would deflect less than the radially laced wheel. As can be seen in Table 3 above, each loading condition had identical maximum deflections across the lacing patterns. Upon further research into the subject, we found that the crossing patterns only assist in adding torsional and lateral stiffness to the wheel. As our model was 2D, we did not have a way to prove that.

Secondly, we expected there to be a much larger change in deflection between the F1 and F2 loading conditions, radial and torsional respectively. Especially when compared to the F3 loading condition that had the largest effect on deflection in the system. We believe the difference between the F1 and F3 conditions comes from a lack of spoke connection where the force is applied in F3. By not having a spoke to transfer the load off the rim, the rim itself must deflect and transfer the energy. This is

confirmed in Figure 10, below, where the dark purple node in the F3 plot is the position of the load whereas the bottom most node in the F1 plot is the position of the load.

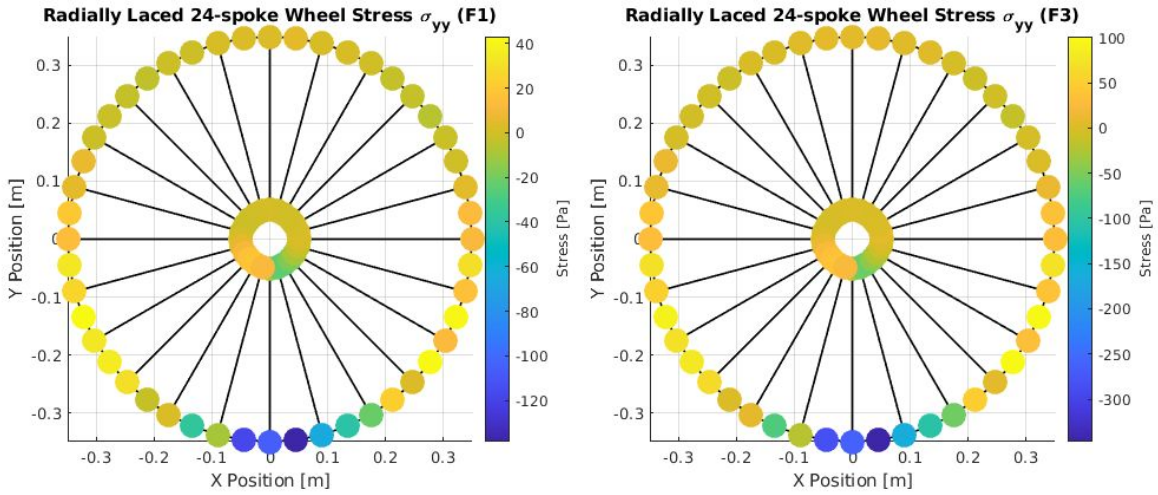

Figure 10: Plot of Sigma_yy in F1 and F3 loading condition (Note the Stress scales)

Finally, in the event of a wheel failure, lots can go wrong. Depending on where the rider is when the wheel fails, it could be as simple as stopping safely at the side of the road. Or, it could be as dangerous as riding off a cliff during the Tour de France. If there is ever something to watch out for when riding or driving, it's the condition of the things that keep you off the ground. Good design of a wheel is critical for the safety of its users and therefore should be kept to the standard software packages with known quality. Our solution was a good learning experience in understanding the requirements of FEM solvers as well as the process of determining shape functions, node mapping, stress analysis, and effective data outputs. This will allow us, in the future, to build more effective FEM models either by hand or in CAD packages.

References:

1. Liu, Xiao-hui & Yan, Bo & Zhang, Hong-yan & Zhou, Song. (2009). Nonlinear numerical simulation method for galloping of iced conductor. Applied Mathematics and Mechanics (English Edition). 30. 489-501. 10.1007/s10483-009-0409-x.